Eleventh USA/Europe Air Traffic Management Research and Development Seminar (ATM2015)

Towards Climate Optimized Flight Trajectories in a Climate Model: AirTraf

Hiroshi Yamashita, Volker Grewe, Patrick Jöckel
Institute of Atmospheric Physics
DLR-German Aerospace Center
Oberpfaffenhofen, Germany
hiroshi.yamashita@dlr.de

Florian Linke
Institute of Air Transportation Systems
DLR-German Aerospace Center
Hamburg, Germany

Martin Schaefer
Institute of Propulsion Technology*
DLR-German Aerospace Center
Cologne, Germany

Daisuke Sasaki
Department of Aeronautics
Kanazawa Institute of Technology
Hakusan, Japan

***Abstract*—Aviation contributes to the anthropogenic climate impact through emissions. Mobility becomes more and more important to society and hence air transportation is expected to grow further over the next decades. Mitigating the climate impact from aviation emissions is needed and a climate compatible air transportation system is required for a sustainable development of commercial aviation. A number of studies suggest avoiding climate sensitive regions by re-routing horizontally and vertically: climate optimized routing. This includes several routing strategies (mitigation options) and shows a great potential for a climate impact reduction, since most of the climate impact arises from non-CO_2 emissions, which are short-lived and vary regionally. This study introduces a new assessment platform AirTraf, which is a simplified model to perform long-term global air traffic simulation in a climate-chemistry model, enabling the assessment of routing strategies. A demonstration of a one-day AirTraf simulation was performed using 103 flight plans for transatlantic flights of Airbus A330 aircraft. The results confirmed that AirTraf simulates the air traffic properly both for flights along the great circle and wind-optimal strategies.**

Keywords-climate impact; aircraft emissions; trajectory optimization

I. INTRODUCTION

Air traffic contributes to the anthropogenic climate impact by emissions of CO_2, NO_x, water vapor, soot, etc. These emissions induce cloudiness and concentration changes of atmospheric constituents. For example, the emissions lead to an increase in the greenhouse gas concentrations of CO_2, ozone and water vapor, and a decrease in that of methane. The emissions also affect induced cloudiness via the formation of contrails, which transform into contrail-cirrus [1]. This changes the terrestrial radiation balances and causes radiative forcing (RF). The RF drives the earth-atmosphere system to a new state of equilibrium through a temperature change. Now the contribution of aviation to the anthropogenic climate impact amounts to roughly 5 % [2, 3]. As the world air traffic still increases (the world annual air traffic growth is + 5 %/year)[4], the anthropogenic impact from aviation is expected to increase further. Mitigating the impact is needed and a climate compatible air transportation system is required for a sustainable development of commercial aviation.

An analysis of the aviation's climate impact is complex. Chemical effects induced by aviation emissions have a number of life-times and thus aviation affects upon the atmosphere range from hours to centuries. A perturbation of CO_2 concentration has a life-time in the order of decades to a century. The atmosphere-ocean system responds to changes in the radiation fluxes in the order of 30 years. Contrails on the other side have a life-time in the order of hours. Thus a long-term simulation is required to estimate aviation's climate impact accurately.

The short-lived effects of aviation, i.e. contrail-cirrus and ozone, largely depend on atmospheric background conditions: the effects depend on the location, altitude and time of the emissions. Contrails form in ice supersaturated regions [5], which are very limited in the spatial extension, with a few 100 m in the vertical and around 150 km horizontally, though with a large variability [6]. Avoiding these regions reduces aviation's contribution to the climate impact via contrail formation drastically. However trade-offs may occur through other components.

Similar effects occur for emissions of nitrogen oxides. Nitrogen oxides, which are emitted in the upper troposphere and lower stratosphere, have life-times ranging from a few days to weeks and months depending on atmospheric transport and chemical background conditions. They have short life-times, when they are emitted in regions, which experience a downward motion, e.g. ahead of a high pressure system. In that

*Present: German Federal Ministry of Transport and Digital Infrastructure

case, NO_x is converted to HNO_3 and then washed out [7]. The climate impact caused by these emissions strongly depends on the local atmospheric conditions.

Recent studies showed a large potential of climate optimized routing to reduce the climate impact of aviation [7, 8, 9]. Other studies investigated systematic changes in routing, i.e. lower flight altitudes combined with a reduced aircraft speed [10, 11]. These studies showed that an altitude change affects the climate impact reduction. In short, climate optimized routing seems to be an effective approach for climate impact reduction. To evaluate the effects quantitatively, however, CO_2-emissions, non-CO_2 emissions, re-routing horizontally and vertically and local atmospheric conditions for flight routes should be considered in a long-term simulation.

If we apply the climate optimized routing to global air traffic, there are two issues. The first is what the optimum route for total climate impact reduction is. Several routing strategies (mitigation options) exist: great circle (minimum flight distance), wind-optimal (minimum flight time), minimum CO_2 emissions, minimum NO_x, contrail avoidance, etc. The second issue is how effective the selected strategy for total climate impact reduction is, particularly in the long term. To develop a common basis for an assessment of strategies, a climate-chemistry model is suitable, which includes an air traffic simulation.

This paper presents the new assessment platform AirTraf. The AirTraf is a simplified global air traffic model coupled to the climate-chemistry model EMAC [12]. An overview, model components and calculation procedures of AirTraf (including trajectory optimization) are presented. Aircraft routing methodologies are also described. To demonstrate AirTraf simulations, a one-day simulation is performed with transatlantic flight plans of Airbus A330 aircraft. The proposed trajectory optimization method is validated, focusing on the trajectory between JFK and MUC. Total values of flight time, fuel-usage, NO_x emission and H_2O emission are compared between different options: great circle at four different altitudes and wind-optimal.

This paper is organized as follows. Section II presents model descriptions and calculation procedures of AirTraf. Section III describes aircraft routing methodologies of great circle and wind-optimal trajectory optimization. Section IV provides a demonstration of a one-day AirTraf simulation. Section V shows an optimization strategy on how a climate-friendly routing can be determined. Finally, Section VI concludes the paper and discusses an outlook for this research.

II. AirTraf: Air Traffic in a Climate Model

A. Overview

AirTraf is a submodel to perform long-term global air traffic simulations in the climate-chemistry model EMAC [12], with flight plans and aircraft/engine data as inputs. With AirTraf, a reduction potential of the climate impact from air traffic by re-routing (horizontally and vertically) can be investigated. The characteristics of AirTraf are as follows.

- Input data for AirTraf are one-day flight plans and aircraft/engine characteristics; output data are flight trajectories and global emission fields. AirTraf can handle an arbitrary number of flight plans.
- EMAC provides meteorological data to AirTraf during long-term simulations. Weather conditions are considered for a flight trajectory calculation, fuel flow and emission calculations.
- AirTraf contains an optimization module to find optimal trajectories based on selected routing strategies (mitigation options).
- AirTraf is parallelized using a message passing interface (MPI) based on a distributed memory approach. Flight trajectories are distributed among the MPI tasks so that each computational core has a similar work load.

As for other common assumptions, AirTraf assumes a spherical Earth (Earth radius is r = 6,371.0 km). Potential conflicts of flight trajectories are ignored. A cruise flight phase is considered, while ground operations, climb and descent flight phases are currently not considered for simplification.

B. Climate-Chemistry Model EMAC

The ECHAM5/MESSy_2.41 Atmospheric Chemistry (EMAC) model [12] is used to perform long-term air traffic simulations considering local atmospheric conditions. The coupling of processes and submodels is organized via the Modular Earth Submodel System (MESSy_2.41 [12]). EMAC simulates the atmosphere from the surface to up to a height of 80 km, i.e. including the troposphere, stratosphere and mesosphere by solving the primitive equations. A variety of submodels enables the coupling of the different components, e.g. radiation, clouds, ocean, chemistry and others. The horizontal and vertical resolution is flexible. Normally, test simulations are performed with a grid resolution of around 500 km and production simulations with 250 km. However, the model also includes the possibility to locally enhance the grid with an embedded regional model with a resolution of up to 7 km.

C. Aviation Data

Fig. 1 shows the flow chart of AirTraf. Aviation data are read during the models' memory initialization phase of EMAC, and the one-day flight plans are distributed among the MPI tasks. The flight plan includes the data on city pairs (airport codes, e.g. JFK-MUC), longitude and latitude values of them, aircraft code and a departure time. If more than a two-day simulation is performed, the one-day flight plan is reused. Oxides of nitrogen emission indices $g(NO_x)/kg(fuel)$ at take off, climb out, approach and idle conditions, and a load factor [13] are provided by ICAO. Aircraft performance data required to calculate the aircraft's fuel flow are provided by EUROCONTROL's Base of Aircraft Data Revision 3.9 (BADA).

D. Calculation Procedures of AirTraf Simulation

A departure check is performed at the beginning of the time

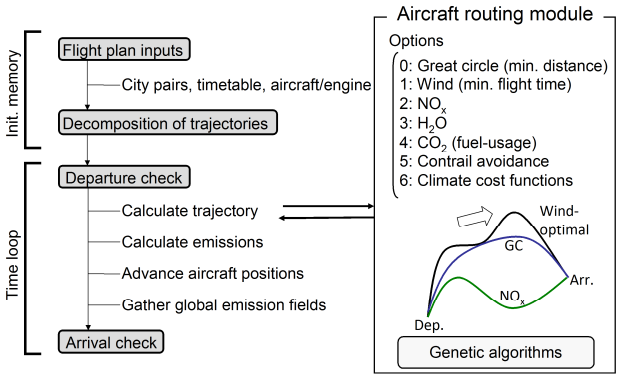

Figure 1. Flowchart of AirTraf.

integration loop of EMAC (see Fig. 1). When an aircraft reaches its departure time, the status of the aircraft is changed into 'in-flight' and the aircraft moves to flying processes. The processes consist of trajectory calculation, emission calculation, advancing the aircraft position and gathering global emission fields. The process of trajectory calculation contains an aircraft routing module, which calculates a flight trajectory for each aircraft. AirTraf will provide seven options: great circle (minimum flight distance), wind-optimal (minimum flight time), nitrogen oxides (NO_x), water vapor (H_2O), fuel-usage (might differ to water vapor, if alternative fuel options are available), contrail avoidance and climate cost functions [14, 15]. If the great circle option is selected, each aircraft flies along a great circle. If another option is selected, a single-objective minimization optimization problem on the option is solved by a Genetic algorithm (GA) [16, 17] including altitude changes, and an optimal trajectory is obtained. For example, if the wind-optimal option is selected, GA finds a wind-optimal trajectory for each aircraft. As for the contrail avoidance option, GA explores the best trajectory for contrail avoidance. The climate cost function is provided by the EU FP7 Project REACT4C [18]. The function can estimate the total climate impact due to several aviation emissions. In the trajectory optimization process, meteorological conditions are provided by EMAC at the departure time of the aircraft. No weather forecasts (or weather archives) are used. The obtained optimal trajectory is not re-optimized in the following time steps of EMAC for simplification. In the present version of AirTraf, the great circle and wind-optimal options are available. The detailed routing methodology of the great circle and wind-optimal options are described in Section III.

After the trajectory calculation process, the obtained trajectory consists of a number of waypoints (arbitrary number), which are equally-spaced along the trajectory. The process of emission calculation (Fig. 1) calculates fuel flow and emissions at the waypoints by a total energy model [19] and using the DLR fuel flow correlation method [20] (Section II.E). In this process, the aircraft weight is calculated at the waypoints. First, the landing weight at the last waypoint (arrival city) is determined using operational empty weight, maximum payload, load factor and 3 % of total fuel usage of the flight. The 3 % amount assumes alternate, reserve and extra fuels. To estimate the total fuel usage roughly (first rough estimation), total flight time calculated by the trajectory calculation process, and fuel consumption values (BADA) corresponding to the mean flight altitude are used. For second accurate estimation, the aircraft weight at the other waypoints (i.e. fuel usage for each segment of waypoints) is calculated iteratively considering weather conditions, and finally the take off weight (at departure city) is determined (the aircraft weight reduces during the flight as fuel is burnt). Here no contingency fuel is considered. After this process, several flight properties are available along the waypoints. They comprise the values of longitude, latitude, altitude, passing time, aircraft ground speed, flight distance, fuel-usage, NO_x and H_2O emissions. If the NO_x option is selected, for example, the processes of trajectory calculation and emission calculation are implemented simultaneously.

As the time integration loop of EMAC progresses, the aircraft flies along the obtained trajectories. The individual aircraft's emissions are gathered into a global emission field. The grid of EMAC consists of a horizontal quadratic Gaussian grid in latitude and longitude. The vertical discretization comprises several layers. The emission values are interpolated onto the nearest grid point of the grid in latitude, longitude and altitude. AirTraf outputs the global fields of NO_x, H_2O, flight distance and fuel-usage.

Finally, an arrival check is performed at the end of every time integration loop. When the aircraft reaches its arrival time, the aircraft quits the flying processes. The status of the aircraft is reset into 'non-flight' (AirTraf considers only a cruise phase).

E. Fuel Flow and Emission Calculations

During the emission calculation process shown in Fig. 1, the fuel flow of the aircraft is calculated by a total energy model according to the BADA methodology (Revision 3.9) [19], while NO_x emissions are obtained by the DLR fuel flow correlation method [20]. Both methods consider effects of aircraft aerodynamic performance of the aircraft, effects of the tailwind/headwind component on an aircraft ground speed, engine performance and meteorological conditions on fuel flow and emissions respectively. The BADA cruise flight model is applied, while climb and descent flight phases are currently not simulated. Note that AirTraf assumes a constant Mach number for the BADA methodology. The emission index of H_2O is 1,230 g(H_2O)/kg(fuel) assuming ideal combustion.

III. AIRCRAFT ROUTING METHODOLOGIES

A. Great Circle Calculation

A great circle module is included in AirTraf, which calculates great circles at an arbitrary flight altitude. A central angle between departure and arrival cities is calculated by the Vincenty formula. The formulae are given as,

$$\Delta\hat{\sigma}_{\mathrm{i}} = \arctan\left(\frac{\sqrt{(\cos\varphi_{\mathrm{a}}\sin\Delta\lambda)^2 + (\cos\varphi_d\sin\varphi_a - \sin\varphi_d\cos\varphi_a\cos\Delta\lambda)^2}}{\sin\varphi_{\mathrm{d}}\sin\varphi_a + \cos\varphi_{\mathrm{d}}\cos\varphi_a\cos\Delta\lambda}\right) \quad (1)$$

$$d_{\mathrm{i}} = (r + h_i)\Delta\hat{\sigma}_i \quad (2)$$

$$d_{\mathrm{i}} = \sqrt{(r+h_i)^2 + (r+h_{i+1})^2 - 2(r+h_i)(r+h_{i+1})\cos\Delta\hat{\sigma}_i} \quad (3)$$

where φ_d and φ_a are values of latitude of departure and arrival city, $\Delta\lambda$ is a difference in longitude of these cities, $\Delta\hat{\sigma}$ is a central angle between these cities, h is a flight altitude of great circle above the sea level (a geopotential altitude is used to determine flight altitudes), d is a great circle distance and n is the number of waypoints ($i = 1,\ldots, n-1$).

To calculate d, either (2) or (3) can be selected. Equation (2) calculates great circles along an arc. Thus if h = constant (e.g. h = FL290; FL290 expresses a flight level at 29,000 ft conventionally), the d calculated by (2) is independent from n. On the other hand, (3) calculates great circles by a linear interpolation between each segment of waypoints based on Polar coordinates. The great circle distance depends on n. The d calculated by (3) becomes close to the value of (2) with an increasing number of waypoints. In AirTraf, an arbitrary number of waypoints can be selected. If AirTraf calculations with the great circle option are compared to those of the wind-optimal (or other) option, an identical number of waypoints should be used with (3). This is because the present trajectory optimization includes altitude changes (see Section III.B).

A true air speed V_{TAS} and a ground speed V_{ground} are defined as,

$$V_{TAS} = M \times a \tag{4}$$

$$V_{ground} = V_{TAS} + V_{wind} \tag{5}$$

where M is a Mach number given by BADA, a is the speed of sound and V_{wind} is the wind component along the flight direction. The values of a and the three-dimensional wind components (u, v, w) are provided for the nearest grid point of EMAC at each waypoint. Thus V_{TAS}, V_{wind} and V_{ground} are calculated at each waypoint (naturally, these values vary with altitude). The flight time is calculated by V_{ground}.

A benchmark test of this module was performed. Great circles were calculated for five city pairs and the results were compared to those of a different tool (Mobvable type script [21]). The test also assessed the sensitivity with respect to the number of waypoints on the great circle distances. The results confirmed that the present module works properly. The details of the benchmark test are described in [22] (unpublished).

B. Wind-optimal Trajectory Calculation

The trajectory optimization is performed using a Genetic Algorithm (GA) [16, 17]. The Adaptive Range Multi-Objective Genetic Algorithm ARMOGA ver.1.2.0 developed by D. Sasaki and S. Obayashi [23, 24, 25] has been integrated in AirTraf as the optimization module. Fig. 2 shows the flowchart of the optimization with GA. GA is an algorithm for optimization problems based on the theory of evolution. An initial population is generated by random numbers. The population evolves over several generations to generate superior individuals by evaluation, selection, crossover and mutation processes. The reason why AirTraf uses GA is that GA is applicable to many types of functions. Several types of

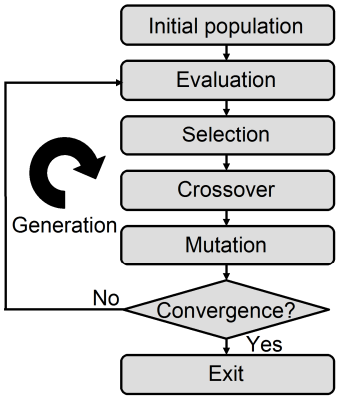

Figure 2. Flowchart of the optimization by the Genetic Algorithm.

functions are integrated in AirTraf as routing options. It is basically not necessary to ensure continuity and differentiability of the functions by use of GA. On the other hand, GA is computationally expensive. A user has to use appropriate settings of optimization parameters (or find a compromise for the settings), since the trajectory optimization is applied for all flight plans in EMAC/AirTraf long-term simulations.

Fig. 3 shows the geometry definition of a trajectory from MUC to JFK, i.e. longitude vs. latitude and longitude vs. altitude. The location of MUC and JFK is fixed; the altitude of them is fixed at FL290. Fig. 3 (top) shows that 3 control points (CP in the black circles) are used. The 3 CPs move independently within the rectangular domains. Centers of the domains are equally-spaced points in longitude between MUC and JFK, and are located on the great circle (diamond symbols). The size of domains is user-defined. Here the short side of the domain is 10 % of the distance in longitude between MUC and JFK; while the long side is 30 % of the distance. Each CP consists of 2 design variables (dv; longitude and latitude values). Totally 6 dvs (dv1 to dv6) are used to create the horizontal projection of the trajectory with a B-spline curve.

From Fig. 3 (bottom), the 5 CPs are used for altitude change. The CPs move independently in altitude direction between FL290 (8,839 m) and FL410 (12,497 m): the altitude change is considered between FL290 and FL410, and an aircraft is freely-movable within the altitude range. This range is a general range for cruise flight of commercial aircraft [9]. The 5 CPs are equally-spaced points in longitude between MUC and JFK. Each CP has 1 dv and totally 5 dvs (dv7 to dv11) are used to create a curve in the longitude and altitude plane with a B-spline curve. Values of altitude are added from the curve to the created trajectory on location using a common value in longitude. The curve and the trajectory are created separately to assure an independency of dvs. Totally 11 dvs are used to express arbitrary trajectories from MUC to JFK.

Initial values of 11 dvs are given by random numbers in the GA processes and trajectory candidates are generated. GA evaluates the present objective function $f(x)$ for each candidate:

$$\textit{Minimize} \qquad f(x) = \sum_{i=1} d_i / V_{ground,i} \left(i = 1,\ldots, n-1\right) \tag{6}$$

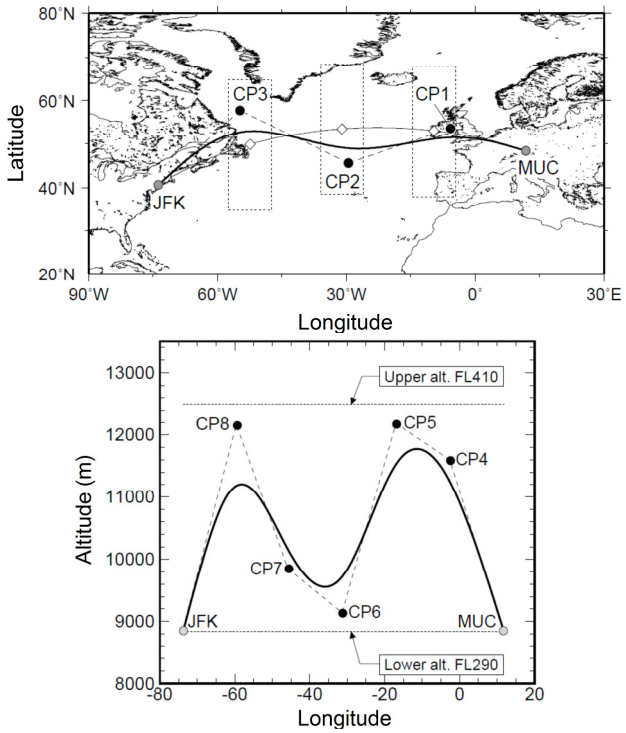

Figure 3. Geometry definition of trajectories. The bold solid line indicates the trajectory between MUC and JFK. Black circles indicate control points. (Top) The thin solid line shows the great circle. The dotted line shows rectangular domains of 3 control points with respect to location. (Bottom) The dotted line shows the domains of 5 control points in altitude.

where d is a flight distance for each segment of waypoints calculated by (3), since an altitude change is included in the trajectory optimization. V_{ground} is the ground speed for each segment calculated by (5) (V_{wind} is calculated in the same way as the great circle option). In short, GA searches a best combination of 11 dvs to minimize $f(x)$.

A benchmark test of the present trajectory optimization method was performed. The single-objective optimization problem on minimization of flight time from MUC to JFK was solved under constant flight speed condition (no-wind) including altitude changes. The results showed that GA found an optimal trajectory, which was nearly identical to the true-optimal solution, and thus the present optimization method is effective for trajectory optimizations. This study also discussed a dependency of initial populations on optimization results, and an appropriate generation number and population size. The details of the benchmark test are described in [22] (unpublished).

IV. Demonstration of a One-Day AirTraf Simulation

A. Calculation Conditions

A one-day air traffic simulation was performed in EMAC with the AirTraf submodel. Both the great circle and wind-optimal options were used. Table I lists the calculation conditions of the simulations. The resolution was T42/L31

TABLE I. Calculation Conditions for One-Day Simulations

AirTraf Option	*Great circle*	*Wind-optimal*
ECHAM5 resolution	T42/L31ECMWF	
Duration of simulation	Jan.01.1978 00:00:00–Jan.02.1978 00:00:00	
Time step	12 min.	
Waypoints	101	
Flight altitude change	Fixed (FL290, FL330, FL370, FL410)	FL290–FL410
Flight plan[a]	103 transatlantic flights (Eastbound 52/Westbound 51)	
Aircraft type	Airbus A330-301	
Engine type	General Electric CF6-80-E1-A2 (1862M39 combustor) × 2	
Mach number	0.82	
Load factor	0.62	
Optimization	N/A	Min. flight time
Design variable (GA)	N/A	11
Generation (GA)	N/A	100
Population (GA)	N/A	100

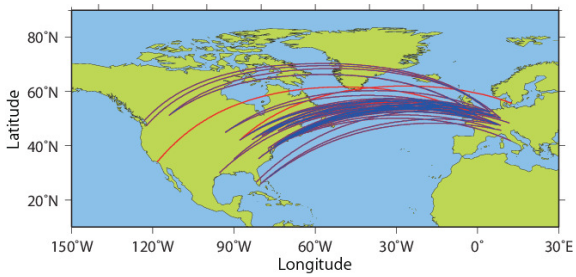

a. provided by the EU FP7 Project REACT4C [18].

Figure 4. The 103 transatlantic flight trajectories used for the one-day simulation (shown by great circles). The flight plans are provided by the EU FP7 Project REACT4C [18]. 52 eastbound flights (red) and 51 westbound flights (blue).

ECMWF (approximately 2.8 degree × 2.8 degree in latitude and longitude). The duration of the simulations was from Jan. 1st 1978 00:00:00 to Jan. 2nd 1978 00:00:00 (UTC). The reason why this date was used is the meteorological condition, which shows a typical weather pattern for winter, including a strong jet stream in the transatlantic region. The 103 transatlantic flight plans (52 eastbound flights and 51 westbound flights) were used. The flight plan was provided by the EU FP7 Project REACT4C [7, 18]. Fig. 4 shows all trajectories used in the one-day simulation. As the transatlantic region is one of the most frequented airspaces in the world, this flight plan is appropriate for the demonstration.

With the great circle option, four simulations were performed separately at FL290, FL330, FL370 and FL410. All flights used the same flight level for this option and the semicircular rule (eastbound/westbound) for the flights was neglected for simplification. With the wind-optimal option, the routing methodology described in Section III.B was used, that

is, all aircraft flew along the minimum flight time routes including altitude changes between FL290 and FL410 (freely-movable). For both options, the number of waypoints was n = 101 (determined by the benchmark test [22]); the flight distance was calculated by (3); the load factor was 0.62, which corresponds to the overall weight load factor in 2008 reported by ICAO [13].

The settings for the optimizations were as follows: the population size was 100; the generation size was 100; Stochastic Universal Sampling [26] was used; Blend crossover (BLX0.2) [27] was used; Polynomial mutation (10 % rate) was used. This optimization was solved with no constraints.

The one-day simulation was parallelized on 4 processing elements (PEs) of Fujitsu Esprimo P900 (Intel Core i5-2500CPU with 3.30 GHz; 4 GB of memory; peak performance of 105.6 × 4 GFLOPS) at the Institute of Atmospheric Physics, DLR. The present simulation required approximately 15 minutes for a great circle case, while it took approximately 20 hours for a wind-optimal case. The computational time is reduced by decreasing the generation number and population size or by using more PEs.

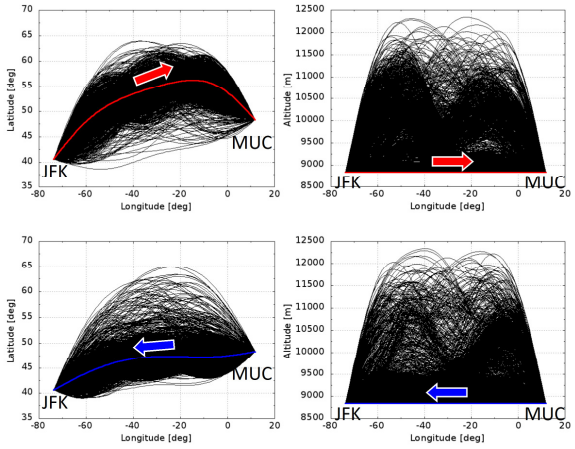

Figure 5. Explored trajectories through trajectory optimizations (black) in the longitude-latitude and in the longitude-altitude planes. (Top) The eastbound flight from JFK to MUC. (Bottom) The westbound flight from MUC to JFK. The red and blue lines indicate the wind-optimal trajectories.

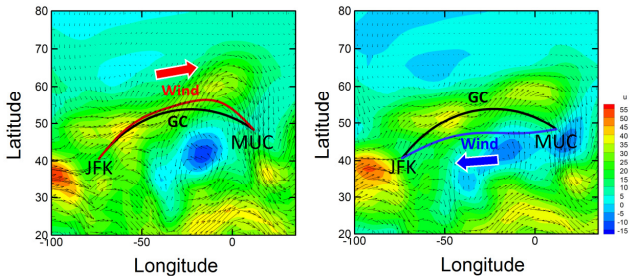

Figure 6. Comparison of the wind-optimal trajectories with wind fields. The contour shows the u m/s wind component at FL290 obtained at each departure time. Arrows (black) show horizontal wind vectors $u + v$. (Left) The red line shows the wind-optimal trajectory from JFK to MUC (the departure time was 01:30:00 UTC). (Right) The blue line shows the wind-optimal trajectory from MUC to JFK (the departure time was 14:27:00 UTC). The black line shows the great circle at FL290.

B. *Optimal Trajectories between JFK and MUC*

To confirm whether the optimization module works properly in EMAC, we focused on the optimization results for eastbound/westbound flights between JFK and MUC, extracted from the one-day simulation with the wind-optimal option. Fig. 5 shows all trajectories explored by the GA (black lines) for location, and in the longitude and altitude plane: (top) eastbound flight from JFK to MUC (the departure time was 01:30:00 UTC); (bottom) westbound flight from MUC to JFK (the departure time was 14:27:00 UTC). From Fig. 5, GA explored diverse trajectories for both flights including altitude change between FL290 and FL410, and found the different wind-optimal trajectories (the red and blue lines). These trajectories were both located at approximately FL290.

Fig. 6 shows a comparison of these optimal trajectories with wind fields. The contour shows the u wind component at FL290 obtained at each departure time. Black arrows show horizontal wind vectors $u + v$. The black line shows the great circle at FL290; and the red and blue lines show the wind-optimal trajectories. In the eastbound case, the optimal trajectory took advantage of the tailwind. In the westbound case, the optimal trajectory avoided the headwind and used the tailwind effectively.

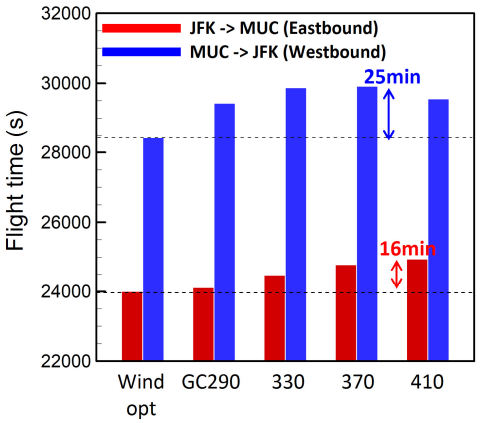

Figure 7. Comparison of the flight time between the wind-optimal case and the four great circle cases (at different flight levels).

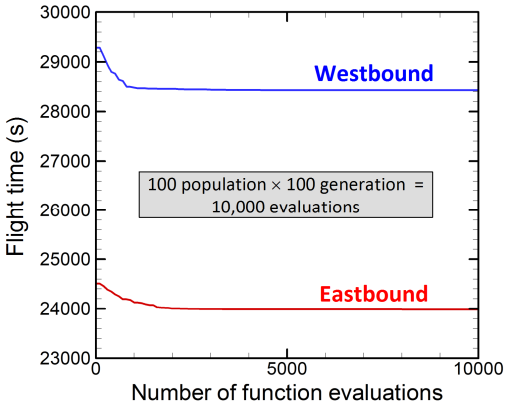

Figure 8. History of convergence of optimizations for both eastbound (from JFK to MUC) and westbound (from MUC to JFK) flights.

Fig. 7 shows a comparison of the flight time between the wind-optimal case and the four great circle cases. It shows that the wind-optimal case leads to reduced flight time compared to the other great circle cases for both eastbound and westbound flights. The maximum reduction in flight time was 945.8 s (in eastbound cases) and 1470.0 s (in westbound cases), respectively. Fig. 8 shows a history of convergence of the optimizations. The horizontal axis shows the number of function evaluations (100 function evaluations correspond to one generation of the GA process). The values converged in both cases. For these two flights (from JFK to MUC, and from MUC to JFK), the presented optimization method found the respective wind-optimal trajectories successfully.

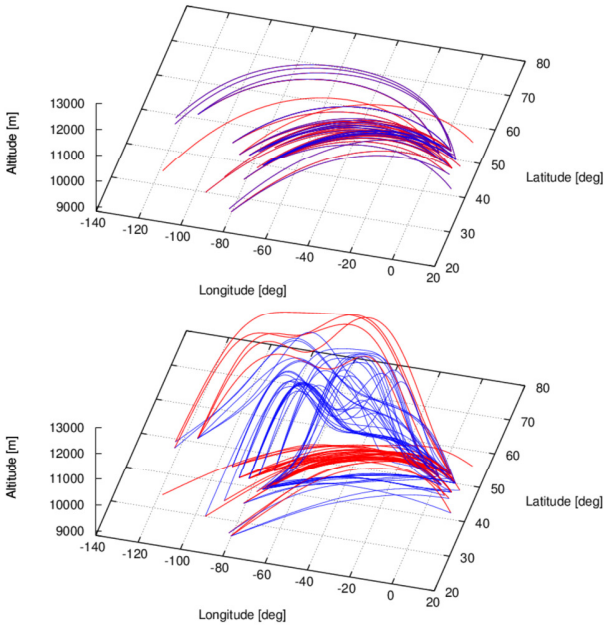

Figure 9. Calculated trajectories from the one-day air traffic simulations. (Top) Great circle at FL290. (Bottom) Wind-optimal case including altitude change between FL290 and FL410. 52 eastbound flights (red) and 51 westbound flights (blue).

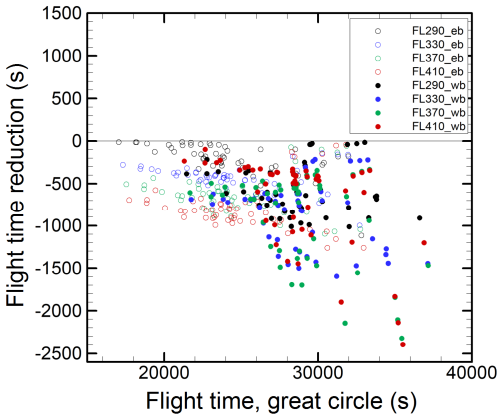

Figure 10. Comparison of the flight time between the wind-optimal case and the four great circle cases. The horizontal axis shows a flight time of great circle case. The vertical axis shows the amount of flight time reduction by wind-optimal option.

C. *Optimal Trajectories for 103 Flights*

Fig. 9 shows all flight trajectories for one-day, calculated with (top) great circle option (FL290) and (bottom) wind-optimal option. The air traffic was simulated correctly just like the flight plans for both cases. The result of the wind-optimal case shows flight altitude changes, as could have been expected. The results also show different flight trajectories for eastbound and westbound flights between the same city pairs, since weather conditions affect the trajectories differently depending on the flight direction (the weather conditions are also different depending on the departure time). The present optimization method found each wind-optimal trajectory.

Fig. 10 shows a comparison of the flight times of the 103 simulated flights between the wind-optimal case and the four great circle cases. The horizontal axis shows the flight time of the great circle case; while the vertical axis shows the flight time reduction by the wind-optimal option. Fig. 10 demonstrates that the wind-optimal option can reduce flight time for all flights. Fig. 11 shows a comparison of the total flight time reduction values for one-day by the wind-optimal option. The red, blue and black bars correspond to the total reduction values of 52 eastbound flights, 51 westbound flights and total 103 flights. The total flight time is reduced in both, eastbound and westbound, cases. Totally the flight time is reduced by −1.5 % to −2.9 %.

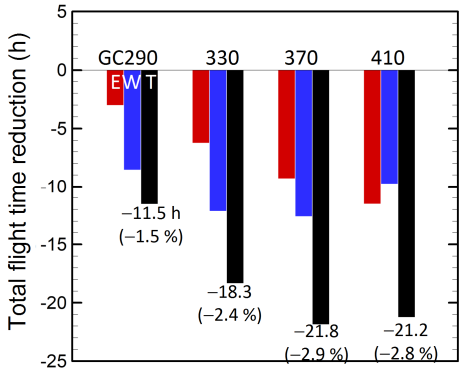

Figure 11. Comparison of the total flight time reduction values for one-day by wind-optimal option: 52 eastbound flights (red), 51 westbound flights (blue) and total 103 flights (black).

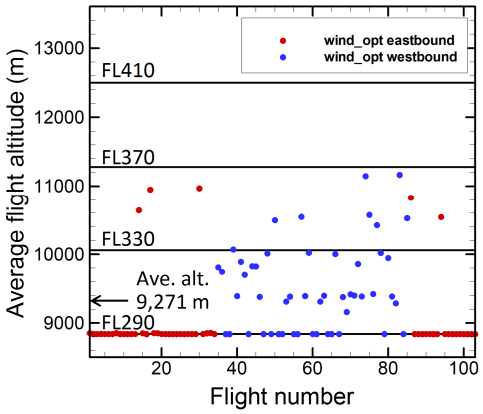

Figure 12. Average flight altitudes of wind-optimal trajectories.

TABLE II. THE MEAN VALUE OF AIRCRAFT SPEEDS CALCULATED USING VALUES OF V_{TAS} AND V_{GROUND} ON ALL WAYPOINTS FOR 52 EASTBOUND AND 51 WESTBOUND FLIGHTS.

Aircraft speed [m/s]	***Flight direction***	***Wind-optimal***	***Great circle***			
			FL290	***FL330***	***FL370***	***FL410***
V_{TAS}	Eastbound	245.1	245.0	242.8	241.3	241.2
	Westbound	245.1	244.8	242.6	241.1	241.1
V_{ground}	Eastbound	268.7	265.3	262.7	260.4	258.7
	Westbound	231.2	223.7	222.0	221.7	223.2

Furthermore, characteristics of the wind-optimal trajectories were examined. Fig. 12 shows a comparison of the average flight altitudes of wind-optimal trajectories. Fig. 12 shows that wind-optimal trajectories are located on comparably low flight altitudes. The average value for 103 flights was 9,271 m (between FL290 and FL330). Table II shows that the mean value of V_{TAS} increases at lower altitudes due to an increase of the speed of sound a (the present simulation assumed a constant Mach number). As a whole, lower flight altitude is appropriate to increase V_{TAS} in the present weather condition. In addition, the mean value of V_{TAS} of wind-optimal case is higher than those of great circle cases for both eastbound and westbound flights. Wind fields also affect the optimizations. Several trajectories are located at higher flight altitudes to take advantage of a tailwind or to avoid a headwind (Fig. 12). In fact, the mean value of V_{ground} of wind-optimal case is higher than those of great circle cases for eastbound and westbound flights (Table II). The altitude change is caused by the variation in V_{TAS} and wind effects. At lower flight altitudes, fuel consumption increases due to an increase of aerodynamic drag. In other words, aircraft has to carry more fuel and thus the aircraft weight increases. Fig. 13 shows a comparison of the average aircraft weights during a flight. The aircraft weight of wind-optimal trajectories becomes heavier on average than those of the great circle cases at FL330, FL370 and FL410.

Finally, global emissions for one-day were compared between the wind-optimal case and the four great circle cases. Fig. 14 shows global distribution maps of the fuel-usage kg(fuel)/box/s (2 hour averages) between the great circle case (FL290) and the wind-optimal case. The results were extracted between 14:00:00 and 20:00:00 (UTC) from the one-day simulation. The maps show that AirTraf simulates fuel-usage caused by air traffic as expected. The maps also show that the higher values of fuel-usage are reduced in the wind-optimal case; however the fuel-usage is spread spatially.

Fig. 15 shows a comparison of the total flight time, total fuel-usage, total NO_x emission and total H_2O emission between the wind-optimal case and the four great circle cases. The wind-optimal case shows the least total flight time in all cases. The wind-optimal case also shows less total fuel-usage, total NO_x and H_2O emissions than those of the great circle at FL290. On the other hand, the wind-optimal case shows more total fuel-usage, total NO_x and H_2O emissions than those of the great circles at FL330, FL370 and FL410. As the wind-optimal trajectories consist of lower flight altitudes (the mean altitude was 9,271 m (between FL290 and FL330)), their fuel consumptions were relatively high. As a result, the total amount of fuel-usage increases and thereby total NO_x emission

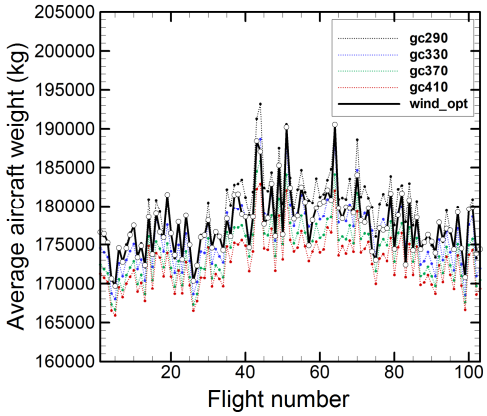

Figure 13. Comparison of the average aircraft weights during the flight.

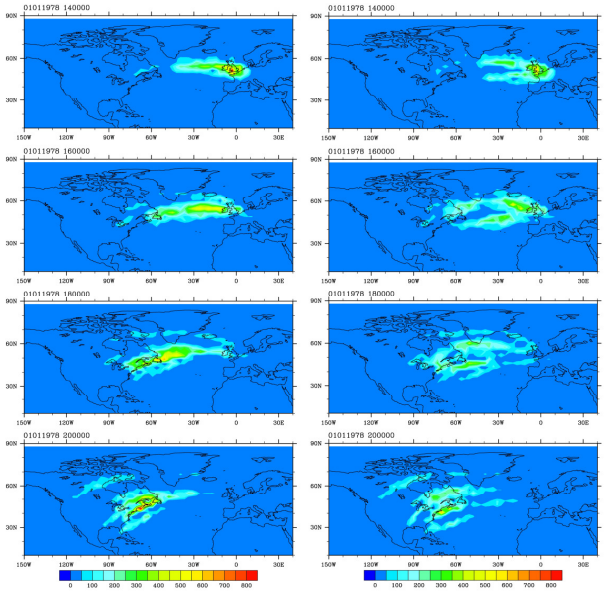

Figure 14. Global vertically integrated distribution of the fuel-usage kg(fuel)/box/s: 2 hour averages calculated from one-day air traffic simulations with EMAC/AirTraf from January 1st 1978 00:00:00 to January 2nd 1978 00:00:00 (UTC). (Left) Great circle at FL290. (Right) Wind-optimal case. The maps, beginning at the top, correspond to the results at 14:00:00; 16:00:00; 18:00:00; 20:00:00.

and H_2O emission increase. Note that the present objective function was the minimization of flight time (not including fuel-usage). These results come from the one-day simulation (i.e. one-day weather condition). It is possible that the trends vary according to atmospheric conditions. It should be investigated carefully how the trends vary for longer time scales.

V. OPTIMIZATION STRATEGY OF AIR TRAFFIC

This section discusses how to develop a strategy for climate-friendly air traffic and a role of AirTraf. The impact of air traffic emissions on the atmosphere and climate has different time-scales (see introduction section). The life-time of contrails is in the order of hours, whereas the life-time of ozone changes is in the order of weeks. Reliable weather forecast is available for a week at most. Hence the direct forecast of all air traffic effects is not possible.

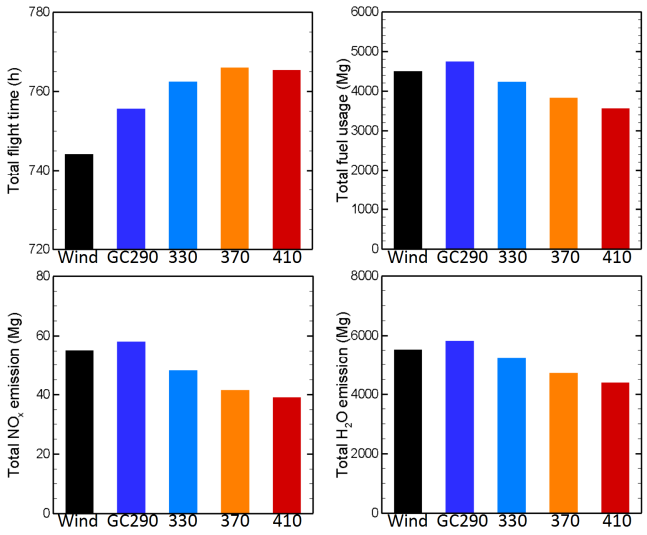

Figure 15. Comparison of the total flight time, total fuel-usage, total NO_x emission and H_2O emission for one-day between the wind-optimal case and the four great circle cases.

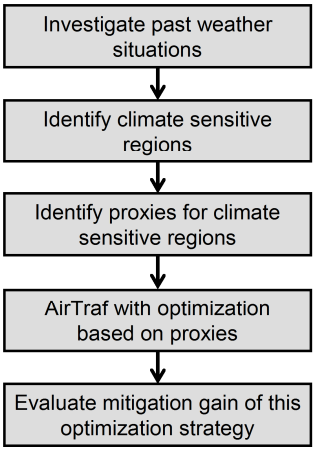

Figure 16. Optimization strategy.

Instead, we propose a multiple step approach. The first step (Fig. 16) is to simulate past weather situations, and especially the impact of locally emitted emissions [7]. These data are called climate cost functions and describe the climate impact of a local emission. A detailed description of this step is given in [28]. These data can then be used to simulate an optimal routing, e.g. as described in [9]. Based on the results from the simulations with locally emitted species, we identify climate sensitive regions (with respect to contrail formation, ozone production etc.) and in a further step we identify proxies, which correlate with the intensity of the climate sensitive regions. These proxies are available in weather forecasts, like temperature, precipitation, ice supersaturated regions, vertical motions or weather pattern in general. The proxies can then be used to optimize air traffic with respect to climate change. An assessment platform is needed to validate the optimization strategy based on these proxies, which is exactly the objective of EMAC/AirTraf. EMAC can be employed to test the optimization strategy in multi-annual simulations and to evaluate the total mitigation gain.

VI. Conclusions and Outlook

Air traffic contributes to the anthropogenic climate impact in the order of 5 %. Mitigation options include numerous approaches. The new assessment platform AirTraf for the ECHAM/MESSy Atmospheric Chemistry (EMAC) model is being developed to simulate long-term global air traffic and to assess the climate impact of routing strategies. AirTraf optimizes flight trajectories according to given routing strategies (options). The great circle and wind-optimal options are available in the present AirTraf.

The one-day air traffic simulation was performed with EMAC/AirTraf using 103 transatlantic flight plans of A330 provided by the EU FP7 Project REACT4C [18]. The results showed that the present optimization module with GA found wind-optimal trajectories for all flights successfully and the module worked properly in AirTraf. The wind-optimal case reduced the total flight time by –1.5 % to –2.9 % for one-day, compared to the other great circle cases. On the other hand, the wind-optimal case showed more fuel-usage and NO_x and H_2O emissions than those of the great circle cases at FL330, FL370 and FL410. It is important to investigate carefully how these trends vary on longer time scales.

The optimization module has been integrated with AirTraf. Air traffic simulations are expected to be performed with other routing options in the future. In addition, AirTraf will be coupled with other submodels of EMAC to convert global emission fields to climate impact metrics.

A comparable study will be performed between AirTraf and Trajectory Calculation Module (TCM) using the same weather patterns, flight plans and aircraft/engine data. The TCM is developed by the Institute of Air Transportation Systems, DLR-Hamburg. TCM can design and analyze new air transportation concepts; TCM can also perform three-dimensional trajectory optimizations.

We also aim to apply AirTraf within a NASA-DLR cooperation, which will include the calculation of climate cost functions [14, 15, 28], the optimization of air traffic according to these climate cost functions for individual days and the long-term evaluation with the EMAC/AirTraf model.

Acknowledgment

The authors wish to thank Prof. Dr. Shigeru Obayashi of the Institute of Fluid Science, Tohoku University for his invaluable comments regarding this work. This work was performed within the DLR Project WeCare.

References

[1] J. E. Penner, D. H. Lister, D. J. Griggs, D. J. Dokken, M. McFarland, (Eds.), Aviation and the global atmosphere, Intergovernmental Panel on Climate Change. Cambridge University Press, Cambridge, UK, 1999.

[2] D. S. Lee, et al., "Transport impacts on atmosphere and climate: aviation," Atmospheric Environment 44, pp. 4678–4734, 2010.

[3] U. Burkhardt and B. Kärcher, "Global rdiative forcing from contrail cirrus," Nature Climate Change 1, pp. 54–58, 2011, doi:10.1038/nclimate1068, http://www.nature.com/nclimate/journal/v1/n1/full/nclimate1068.html.

[4] D. S. Lee et al., "Aviation and global climate change in the 21st century," Atmospheric Environment 43, pp. 3520–3537, 2009.

[5] U. Schumann, “On conditions for contrail formation from aircraft exhausts,” Meteorol. Z. 5, pp. 4–23, 1996.

[6] P. Spichtinger, K. Gierens, U. Leiterer, H. Dier, “Ice supersaturation in the tropopause region over Lindenberg,” Germany, Meteorol. Z. 12, pp. 143–156, 2003.

[7] S. Matthes, U. Schumann, V. Grewe, C. Frömming, K. Dahlmann, A. Koch, H. Mannstein, Climate Optimized Air Transport, Ed. U. Schumann, Springer Heidelberg New York Dordrecht London, 2012, pp. 727–746, ISBN 978-3-642-30182-7, ISBN 978-3-642-30183-4 (eBook), doi 10.1007/978-3-642-30183-4.

[8] U. Schumann, K. Graf and H. Mannstein, “Potential to reduce the climate impact of aviation by flight level changes,” 3rd AIAA Atmosphere Space Environments Conference, AIAA Paper 2011-3376, Honolulu, Hawaii, 2011.

[9] B. Sridhar, N. Y. Chen and H. K. Ng, “Energy efficient concepts for reducing the environmental impact of aviation,” Tenth USA/Europe Air Traffic Management Research and Development Seminar 2013, 2013.

[10] C. Frömming, M. Ponater, K. Dahlmann, V. Grewe, P. D. S. Lee and R. Sausen, “Aviation-induced radiative forcing and surface temperature change in dependency of the emission altitude,” J. Geophys. Res.,117, D19, 2012, doi:10.1029/2012JD018204.

[11] A. Koch, B. Lührs, K. Dahlmann, F. Linke, V. Grewe, M. Litz, M. Plohr, B. Nagel, V. Gollnick and U. Schumann, “Climate impact assessment of varying cruise flight altitudes applying the CATS simulation approach,” 3rd CEAS Air Space Conference, 2011.

[12] P. Jöckel, A. Kerkweg, A. Pozzer, R. Sander, H. Tost, H. Riede, A. Baumgaertner, S. Gromov and B. Kern, “Development cycle 2 of the Modular Earth Submodel System (MESSy2),” Geosci. Model Dev., 3, pp. 717–752, 2010, doi:10.5194/gmd-3-717-2010, http://www.geosci-model-dev.net/3/717/2010/.

[13] P. Anthony, “The fuel factor,” ICAO Journal, 64, 12, 2009.

[14] V. Grewe, C. Frömming, S. Matthes, S. Brinkop, M. Ponater, S. Dietmüller, P. Jöckel, H. Garny, E. Tsati, K. Dahlmann, et al., “Aircraft routing with minimal climate impact: the REACT4C climate cost function modelling approach (V1.0),” Geoscientific Model Development, 7, pp. 175–201, 2014.

[15] V. Grewe, T. Champougny, S. Matthes, C. Frömming, S. Brinkop, O. A. Søvde, E. A. Irvine, L. Halscheidt, “Reduction of the air traffic's contribution to climate change: a REACT4C case study,” Atmospheric Environment, 94, pp. 616–625, 2014.

[16] J. H. Holland, Adaptation in natural and artificial systems, University of Michigan Press, 1975.

[17] D. E. Goldberg, Genetic algorithms in search, optimization and machine learning, Addison Wesley, 1989.

[18] Reducing Emissions from Aviation by Changing Trajectories for the benefit of Climate, EU FP7 Project REACT4C. http://www.react4c.eu.

[19] M. Schaefer, “Development of a forecast model for global air traffic emissions,” Doctoral dissertation, Ruhr-Universität Bochum, pp. 27–29, 2012.

[20] F. Deidewig, A. Döpelheuer, M. Lecht, “Methods to assess aircraft engine emissions in flight,” International Council of the Aeronautical Sciences, 4.1.2, pp. 1–11, 1996.

[21] Mobvable type script, http://www.movable-type.co.uk/scripts/latlong.html.

[22] H. Yamashita, V. Grewe, P. Jöckel, F. Linke, M. Schaefer, D. Sasaki, “Development of AirTraf submodel in EMAC (tentative),” unpublished, (in preparation for Geosci. Model Dev.).

[23] D. Sasaki, S. Obayashi and K. Nakahashi, “Navier-stokes optimization of supersonic wings with four objectives using evolutionary algorithm,” Journal of Aircraft, Vol. 39, No. 4, pp. 621−629, 2002.

[24] D. Sasaki and S. Obayashi, “Development of efficient multi-objective evolutionary algorithms: ARMOGAs (adaptive range multi-objective genetic algorithms),” The reports of the Institute of Fluid Science, Tohoku University, Vol. 16, pp. 11−18, 2004.

[25] D. Sasaki and S. Obayashi, “Efficient search for trade-offs by adaptive range multi-objective genetic algorithms,” Journal of Aerospace Computing, Information, and Communication, Vol. 2, pp. 44−64, 2005.

[26] J. E. Baker, “Adaptive selection methods for genetic algorithms,” International Conference on Genetic Algorithms and Their Applications, pp. 101−111, 1985.

[27] L. J. Eshelman and J. D. Schaffer, “Real-coded genetic algorithms and interval-schemata,” In Foundations of Genetic Algorithms 2 (FOGA-2), pp. 187−202, 1993.

[28] C. Frömming, V. Grewe, P. Jöckel, S. Brinkop, S. Dietmüller, H. Garny, M. Ponater, E. Tsati, S. Matthes, “Climate cost functions as basis for climate optimized flight trajectories,” Tenth USA/Europe Air Traffic Management Research and Development Seminar 2013, 2013.

AUTHOR BIOGRAPHY

Dr. Hiroshi Yamashita studied mechanical engineering at Tohoku University (Japan, 2004, Diploma) and system information sciences at Tohoku University (Japan, 2009, PhD). He worked as a postdoctoral fellow in the fields of supersonic aircraft design and sonic boom simulations at the Institute of Fluid Science, Tohoku University in 2009-2011. He became a research fellow of the Japan Society for the Promotion of Science and visited DLR-Institut für Physik der Atmosphäre (Germany) in 2011-2013. Since 2013 he works at DLR regarding aviation and climate impacts. Dr. Yamashita is a member of American Institute of Aeronautics and Astronautics and Japan Society for Aeronautical and Space Sciences.

Dr. Volker Grewe studied mathematics at the University Augsburg (diploma), Germany and meteorology at the Ludwig-Maximilians-University in Munich (Germany). He has working as a scientist in the field of climate-chemistry interactions with focus on traffic and air traffic effects upon the atmosphere since 1992 at the DLR-Oberpfaffenhofen. He also worked at NASA-GISS in New York 1999-2000 and visited NCAR (Boulder, CO) NASA-Ames, NASA-GISS and CICERO (Oslo, Norway) during sabbaticals as a guest scientist. Since 2014 he is visiting professor at the TU Delft. He is topical editor of the journal Geoscientific Model Development (www.geoscientific-model-development.net).

Dr. Patrick Jöckel received his Diploma in physics from the Technische Universität Darmstadt, Germany and his PhD in natural and mathematical sciences from the University of Heidelberg, Germany. He coordinates the multi-institutional development and evaluation of the Modular Earth Submodel System (MESSy). In 2005 he received the Heinz Billing Award for the Advancement of Scientific Computation. He is an editor of the journal Atmospheric Chemistry and Physics, and Geoscientific Model Development. He worked at the Max-Planck-Institute of Chemistry in Mainz, Germany for many years. Since 2009 he works at the DLR-Institute for Atmospheric Physics.

Mr. Florian Linke is Head of Department of “Air Traffic Infrastructures and Processes” at the DLR Air Transportation Systems, Hamburg, Germany. He received his diploma in Aeronautical Engineering from RWTH Aachen University in 2007. Mr. Linke has a background in Air Traffic Management and flight mechanics, guidance and control and now focuses on trajectory optimization and new operational concepts to reduce the environmental impact of aviation. He is currently doing his Ph.D. at Hamburg University of Technology. Mr. Linke is a member of the American Institute of Aeronautics and Astronautics.

Dr. Martin Schaefer graduated from Technische Universität Berlin in 2006 as an Aeronautical Engineer with specialisation in air transport. From 2006 to 2013 he worked as a Research Engineer at the DLR Institute of Propulsion Technology with a focus on aircraft engine emissions and aviation scenarios. Since 2012 he holds a doctoral degree in Engineering from Ruhr-Universität Bochum. In 2013 he joined the German Federal Ministry of Transport and Digital Infrastructure as a Technical Advisor on Aviation’s Environmental Impacts.

Dr. Daisuke Sasaki is an assistant professor at Department of Aeronautics at Kanazawa Institute of Technology since 2012. He received his BSc and MSc in Aerospace Engineering and his PhD in Information Science in the field of aerodynamic design optimization from Tohoku University. After his PhD, he worked at University of Southampton and Cambridge University for the research project with Rolls-Royce plc. He then worked at Department of Aerospace Engineering, Tohoku University as an assistant professor for CFD development and aerodynamic design systems. He is currently working on various aerospace projects in the fields of design optimization and CFD.